PTEP

Prog. Theor. Exp. Phys. **2013**, 093A02 (11 pages)
DOI: 10.1093/ptep/ptt070

Three-torus-causing mechanism in a third-order forced oscillator

Kaoru Itoh[1,*], Naohiko Inaba[2], Munehisa Sekikawa[3], and Tetsuro Endo[1]

[1]*Department of Electronics and Bioinformatics, Meiji University, Kawasaki 214-8571, Japan*
[2]*Organization for the Strategic Coordination of Research and Intellectual Property, Meiji University, Kawasaki 214-8571, Japan*
[3]*Institute of Industrial Science, the University of Tokyo, Tokyo 153-8505, Japan*
[*]E-mail: ce31006@meiji.ac.jp

Received April 18, 2013; Revised July 22, 2013; Accepted July 26 2013; Published September 1, 2013

In this paper, we discuss the bifurcation of a limit cycle to a three-torus in a piecewise linear third-order forced oscillator. A three-torus cannot be generated in third-order autonomous oscillators; our dynamical model exhibits a three-torus of minimal dimension. We adopt a third-order piecewise linear oscillator that exhibits a two-torus and apply a periodic perturbation to this oscillator. First, appropriate parameter values are selected to induce a limit cycle in the oscillator. In addition, this limit cycle is synchronized to the periodic perturbation. When the angular frequency of the periodic perturbation decreases, the oscillator is desynchronized, and a two-torus appears via a saddle-node bifurcation. This was verified by tracking the fixed point corresponding to the limit cycle on the Poincaré map and calculating the eigenvalues of the fixed point. Furthermore, the variation of a bifurcation parameter results in the generation of a three-torus via a quasi-periodic Neimark–Sacker bifurcation. This bifurcation is identified as a quasi-periodic Neimark–Sacker bifurcation from the observation of the second and third degenerate negative Lyapunov exponents. It was confirmed that all of the three Lyapunov exponents become zero at the quasi-periodic Neimark–Sacker bifurcation point.

Subject Index A30

1. Introduction

The recent increase in computational power has enabled the analyses of higher-order dynamical systems and has naturally attracted considerable attention [1–4,6,7,9–19]. Such higher-order dynamical systems exhibit notable phenomena, such as torus doubling [1], hyperchaos [3], and three-tori [4–17]. These phenomena are not observed in low-order systems, such as second-order nonautonomous oscillators and third-order autonomous oscillators. In particular, in recent years, the bifurcations relevant to the three-torus have been a subject of intensive research [4–19].

Both numerical simulations and experimental measurements have been conducted for three-coupled oscillators, and the observations indicated a three-torus [4,12]. However, these oscillators were not minimal dimensional oscillators that generate a three-torus. We are therefore interested in three-torus generating oscillators of minimal dimension. It has been shown that a class of fourth-order autonomous oscillators can have a three-torus near the codimension-two bifurcation point called the Hopf–Hopf bifurcation [8,9]. Such oscillators are dynamics of minimal dimension generating a three-torus as autonomous ODEs. In contrast, third-order nonautonomous oscillators under weak

periodic perturbation could generate a three-torus because third-order autonomous oscillators can exhibit a two-torus [20,21]. However, the bifurcation scenario from a limit cycle to a three-torus in such nonautonomous oscillators has not yet been investigated.

In this paper, we discuss a mechanism that causes a three-torus in a third-order piecewise linear forced oscillator. We adopt the third-order piecewise linear autonomous circuit proposed by Matsumoto et al. [20] as a two-torus-generating circuit of minimal dimension and apply a periodic perturbation to this oscillator. In the analysis, we employ explicit solutions of the piecewise dynamical equations and their variational forms because the bifurcation transition from a limit cycle to a three-torus occurs under sensitive circumstances. We must solve the equations numerically when the solution crosses the boundary of each piecewise linear branch. These equations are not approximated; therefore, these equations can be solved to any degree of precision using a computer. In an actual calculation procedure, they are solved with an accuracy of 10^{-15}.

Alaggio and Rega asserted that a three-torus occurs as a consequence of two Neimark–Sacker (Hopf) bifurcations [16]. However, this appears to be incorrect. Fujiwara et al. clearly demonstrated using simple and natural discrete dynamics that the second Neimark–Sacker bifurcation point does not agree with the bifurcation boundary at which a two-torus bifurcates to a three-torus [19]. Vitoro et al. call such a bifurcation boundary from a two-torus to a three-torus a quasi-periodic Neimark–Sacker bifurcation [18]. In our model, the bifurcation transition from a limit cycle to a three-torus does not occur as a consequence of a Neimark–Sacker bifurcation and a quasi-periodic Neimark–Sacker bifurcation because the Poincaré map is of the third order. First, the angular frequency of the periodic perturbation is equalized to the natural angular frequency of the limit cycle of the oscillator so that the oscillator is synchronized to the forcing term. Actually, synchronization is confirmed. As the angular frequency decreases, the oscillator is desynchronized by a saddle-node bifurcation, and a quasi-periodic solution (a two-torus) is generated. The generation of the saddle-node bifurcation is confirmed by checking the eigenvalues of the fixed point of the Poincaré map. The generation of the quasi-periodic oscillation is verified by calculating the Lyapunov exponents. Before the saddle-node bifurcation, the Poincaré map has one real eigenvalue approximately equal to 1 and a pair of complex-conjugate eigenvalues inside the unit circle. The fixed point on the Poincaré map disappears at the saddle-node bifurcation point. The largest Lyapunov exponent becomes zero after this bifurcation. Note that the second and third Lyapunov exponents take the same negative value, although the fixed point disappears owing to the saddle-node bifurcation. Therefore, the nature of the pair of complex-conjugate eigenvalues remains in the attractor after the saddle-node bifurcation.

As the bifurcation parameter is varied further, the two-torus bifurcates to a three-torus via a quasi-periodic Neimark–Sacker bifurcation. At this bifurcation point, all three Lyapunov exponents become zero. The bifurcation from the two-torus to a three-torus is identified as a quasi-periodic Neimark–Sacker bifurcation because the second and third Lyapunov exponents are degenerate before the bifurcation [5,12]. In addition, the bifurcation structure of a two-torus Arnold tongue [12] is observed in a three-torus-generating region.

2. Circuit set-up and exact solution of the piecewise linear system

Figure 1 shows the circuit diagram analyzed in this study in which the capacitance of the right capacitor is a negative value $-C_1$. In the figure, if $b_1 = 0$, the circuit is identical to the two-torus generating oscillator proposed by Matsumoto et al. [20]. The governing equation of the circuit is represented by

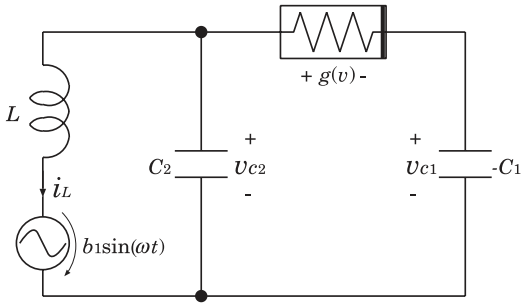

Fig. 1. Circuit diagram.

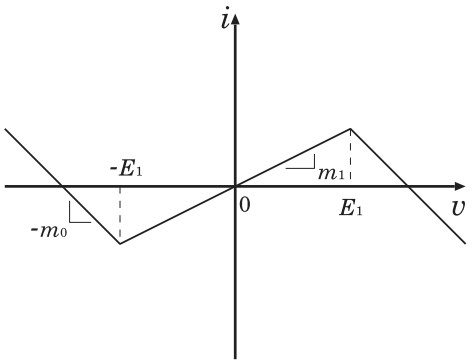

Fig. 2. $v - i$ characteristics of the piecewise linear nonlinear register $i = g(v)$.

the following third-order nonautonomous ordinary differential equation.

$$\begin{aligned} C_1\frac{\mathrm{d}v_{C_1}}{\mathrm{d}t} &= -g(v_{C_2} - v_{C_1}),\\ C_2\frac{\mathrm{d}v_{C_2}}{\mathrm{d}t} &= -g(v_{C_2} - v_{C_1}) - i_L,\\ L\frac{\mathrm{d}i_L}{\mathrm{d}t} &= v_{C_2} + b_1\sin(\omega t), \end{aligned} \tag{2.1}$$

where $g(\cdot)$ is a nonlinear term, which is represented by the following three-segment piecewise linear function.

$$g(v) = -m_0 v + 0.5(m_0 + m_1)[|v + E_1| - |v - E_1|]. \tag{2.2}$$

Figure 2 shows the $v - i$ characteristics of the nonlinear function $g(v)$.

By changing each variable and constant as

$$\begin{aligned} &x = v_{C_1}/E_1, \quad y = v_{C_2}/E_1, \quad z = i_L/C_2E_1, \quad \alpha = C_2/C_1,\\ &\beta = 1/LC_2, \quad a = m_0/C_2, \quad b = m_1/C_2, \quad B = b_1/LC_2E_1, \end{aligned} \tag{2.3}$$

the normalized equation is derived as follows.

$$\dot{x} = -\alpha f(y - x), \quad \dot{y} = -f(y - x) - z, \quad \dot{z} = \beta y + B\sin(\omega t), \tag{2.4}$$

where

$$f(u) = -au + 0.5(a + b)(|u + 1| - |u - 1|). \tag{2.5}$$

The circuit dynamics depends on the six parameters α, β, B, ω, a, and b. We set a, b, and β as

$$a = 0.07, \quad b = 0.1, \quad \beta = 1. \tag{2.6}$$

These parameter values are the same as those used by Matsumoto et al. [20].

Because the circuit dynamics is piecewise linear, the explicit solutions in each piecewise linear branch are obtained. Let δ_1 and $\lambda_1 \pm i\gamma_1$ be the roots of the eigenequation in the region $y - x > 1$ and $y - x < -1$. Further, let δ_2 and $\lambda_2 \pm i\gamma_2$ be the roots of the eigenequation in the region $-1 < y - x < 1$. Then, the piecewise linear solutions in each region are expressed by the following equations. If $y - x > 1$ (Region 1)

$$\begin{bmatrix} x(t) \\ y(t) \\ z(t) \end{bmatrix} = F_1(t - t_0) \times \begin{bmatrix} A_1 \\ B_1 \\ C_1 \end{bmatrix} + G_1(t), \tag{2.7}$$

$$F_1(t) = \begin{bmatrix} f_{x1}(t) \\ f_{y1}(t) \\ f_{z1}(t) \end{bmatrix}, \quad G_1(t) = \begin{bmatrix} g_{x1}(t) \\ g_{y1}(t) \\ g_{z1}(t) \end{bmatrix}$$

$$f_{x1}(t) = (\mathrm{e}^{\lambda_1 t}\, \mathrm{e}^{\delta_1 t} \sin(\gamma_1 t)\, \mathrm{e}^{\delta_1 t} \cos(\gamma_1 t)),$$

$$g_{x1}(t) = -\frac{a+b}{a} + k_{11} \sin(\omega t) + k_{21} \cos(\omega t),$$

$$f_{y1}(t) = -\frac{1}{\alpha a}\frac{\mathrm{d}}{\mathrm{d}t} f_{x1}(t) + f_{x1}(t),$$

$$g_{y1}(t) = -\frac{1}{\alpha a}\frac{\mathrm{d}}{\mathrm{d}t} g_{x1}(t) + g_{x1}(t) + \frac{b}{a} + 1,$$

$$f_{z1}(t) = -\frac{\mathrm{d}}{\mathrm{d}t} f_{y1}(t) + a f_{y1}(t) - a f_{x1}(t),$$

$$g_{z1}(t) = -\frac{\mathrm{d}}{\mathrm{d}t} g_{y1}(t) + a g_{y1}(t) - a g_{x1}(t) - a - b,$$

$$k_{11} = \frac{B\omega(k_{41}\omega + k_{31}a(\alpha - 1))}{k_{31}^2 + k_{41}^2},$$

$$k_{21} = \frac{B\omega(k_{31}\omega - k_{41}a(\alpha - 1))}{k_{31}^2 + k_{41}^2},$$

where

$$k_{32} = -\omega(\omega^2 - \beta), \quad k_{42} = a(-\alpha\beta + \omega^2(\alpha - 1)),$$

where A_1, B_1, and C_1 are constants that satisfy the initial condition $(t, x, y, z) = (t_0, x_0, y_0, z_0)$. They are explicitly given by

$$\begin{bmatrix} A_1 \\ B_1 \\ C_1 \end{bmatrix} = F_1(0)^{-1} \times \left\{ \begin{bmatrix} x_0 \\ y_0 \\ z_0 \end{bmatrix} - G_1(t_0) \right\}. \tag{2.8}$$

If $|y - x| \leq 1$ (Region 2)

$$\begin{bmatrix} x(t) \\ y(t) \\ z(t) \end{bmatrix} = F_2(t - t_0) \times \begin{bmatrix} A_2 \\ B_2 \\ C_2 \end{bmatrix} + G_2(t), \tag{2.9}$$

$$F_2(t) = \begin{bmatrix} f_{x2}(t) \\ f_{y2}(t) \\ f_{z2}(t) \end{bmatrix}, \quad G_2(t) = \begin{bmatrix} g_{x2}(t) \\ g_{y2}(t) \\ g_{z2}(t) \end{bmatrix}$$

$$f_{x2}(t) = (\mathrm{e}^{\lambda_2 t}\, \mathrm{e}^{\delta_2 t} \sin(\gamma_2 t)\, \mathrm{e}^{\delta_2 t} \cos(\gamma_2 t)),$$

$$g_{x2}(t) = k_{12} \sin(\omega t) + k_{22} \cos(\omega t),$$

$$f_{y2}(t) = -\frac{1}{\alpha b} \frac{\mathrm{d}}{\mathrm{d}t} f_{x2}(t) + f_{x2}(t),$$

$$g_{y2}(t) = -\frac{1}{\alpha b} \frac{\mathrm{d}}{\mathrm{d}t} g_{x2}(t) + g_{x2}(t),$$

$$f_{z2}(t) = -\frac{\mathrm{d}}{\mathrm{d}t} f_{y2}(t) - b f_{y2}(t) + b f_{x2}(t),$$

$$g_{z2}(t) = -\frac{\mathrm{d}}{\mathrm{d}t} g_{y2}(t) - b g_{y2}(t) + b g_{x2}(t),$$

$$k_{12} = \frac{B\omega(k_{42}\omega - k_{32} b(\alpha - 1))}{k_{32}^2 + k_{42}^2},$$

$$k_{22} = \frac{B\omega(k_{32}\omega + k_{42} b(\alpha - 1))}{k_{32}^2 + k_{42}^2},$$

where

$$k_{32} = -\omega(\omega^2 - \beta), \quad k_{42} = b(\alpha\beta - \omega^2(\alpha - 1)),$$

$$\begin{bmatrix} A_2 \\ B_2 \\ C_2 \end{bmatrix} = F_2(0)^{-1} \times \left\{ \begin{bmatrix} x_0 \\ y_0 \\ z_0 \end{bmatrix} - G_2(t_0) \right\}. \tag{2.10}$$

If $y - x < 1$ (Region 3)

$$\begin{bmatrix} x(t) \\ y(t) \\ z(t) \end{bmatrix} = F_3(t - t_0) \times \begin{bmatrix} A_3 \\ B_3 \\ C_3 \end{bmatrix} + G_3(t), \tag{2.11}$$

$$F_3(t) = \begin{bmatrix} f_{x3}(t) \\ f_{y3}(t) \\ f_{z3}(t) \end{bmatrix}, \quad G_3(t) = \begin{bmatrix} g_{x3}(t) \\ g_{y3}(t) \\ g_{z3}(t) \end{bmatrix}$$

$$f_{x3}(t) = (\mathrm{e}^{\lambda_1 t}\, \mathrm{e}^{\delta_1 t} \sin(\gamma_1 t)\, \mathrm{e}^{\delta_1 t} \cos(\gamma_1 t)),$$

$$g_{x3}(t) = \frac{a + b}{a} + k_{13} \sin(\omega t) + k_{23} \cos(\omega t),$$

$$f_{y3}(t) = -\frac{1}{\alpha a} \frac{\mathrm{d}}{\mathrm{d}t} f_{x3}(t) + f_{x3}(t),$$

$$g_{y3}(t) = -\frac{1}{\alpha a} \frac{\mathrm{d}}{\mathrm{d}t} g_{x3}(t) + g_{x3}(t) - \frac{b}{a} - 1,$$

$$f_{z3}(t) = -\frac{\mathrm{d}}{\mathrm{d}t} f_{y3}(t) + a f_{y3}(t) - a f_{x3}(t),$$
$$g_{z3}(t) = -\frac{\mathrm{d}}{\mathrm{d}t} g_{y3}(t) + a g_{y3}(t) - a g_{x3}(t) + a + b,$$
$$k_{13} = \frac{B\omega(k_{43}\omega + k_{33}a(\alpha - 1))}{k_{33}^2 + k_{43}^2},$$
$$k_{23} = \frac{B\omega(k_{33}\omega - k_{43}a(\alpha - 1))}{k_{33}^2 + k_{43}^2},$$

where

$$k_{33} = -\omega(\omega^2 - \beta), \quad k_{43} = a(-\alpha\beta + \omega^2(\alpha - 1)),$$
$$\begin{bmatrix} A_3 \\ B_3 \\ C_3 \end{bmatrix} = F_3(0)^{-1} \times \left\{ \begin{bmatrix} x_0 \\ y_0 \\ z_0 \end{bmatrix} - G_3(t_0) \right\}. \tag{2.12}$$

To plot the attractors of Eq. (2.4), the state variables $x(t; t_0, x_0, y_0, z_0)$, $y(t; t_0, x_0, y_0, z_0)$, and $z(t; t_0, x_0, y_0, z_0)$ must be connected continuously at the boundaries between Regions 1, 2, and 3, respectively. For example, when the solution in Region 2 hits the boundary $y - x = 1$ at $t = t_1$, t_1 is derived by solving the following equation:

$$[-1\ 1\ 0] \times F_2(t_1 - t_0) \times \begin{bmatrix} A_2 \\ B_2 \\ C_2 \end{bmatrix} + G_2(t_1) - 1 = 0. \tag{2.13}$$

Note that Eq. (2.13) includes no approximation. Therefore, Eq. (2.13) can be solved to any degree of precision by using a computer. In this study, Eq. (2.13) is solved with an accuracy of 10^{-15}.

Because the exact solutions are given by Eqs. (2.7), (2.9), and (2.11), the obtained solution does not depend on the integration step-size h. However, this piecewise linear system is required to be carefully solved. Figure 3 shows a schematic illustration of the piecewise linear solutions. We assume that when $t = t_1$, $y - x$ is less than 1 in Fig. 3(a). This point is denoted by Q_1. If $y - x$ is greater than 1 at $t = t_1 + h$, as indicated by the point Q_2, the boundary condition can be appropriately solved; $y - x = 1$ can be exactly solved, and the point P_1 in Fig. 3(a) is obtained with an accuracy of 10^{-15}. However, the case illustrated in Fig. 3(b) is also a possibility. As shown in this figure, the genuine solution reaches the threshold $y - x = 1$. However, the computed solution with step-size h does not cross the threshold $y - x = 1$, i.e., both Q_1' and Q_2' in Fig. 3(b) are under $y - x = 1$. This case causes a critical numerical error. Such a situation occurs because the objective attractors are tori. Thus, to prevent this error, we check all extreme values $y - x$ by solving $\dot{y} - \dot{x} = 0$ with an accuracy of 10^{-15}. For example, our code calculated the maximum value P_2, as shown in Fig. 3(c).

Figure 4 shows the attractor in the absence of perturbation ($B = 0$). Figure 4(a) shows a limit cycle, while Fig. 4(b) shows a two-torus.

3. Mechanism causing a three-torus in the oscillator under weak periodic perturbation

Because a two-torus is generated by the circuit dynamics of Eq. (2.4) at $B = 0$, Eq. (2.4) can generate a three-torus with a positive value of B. In this section, we investigate the bifurcation scenario for the transition of a limit cycle to a three-torus.

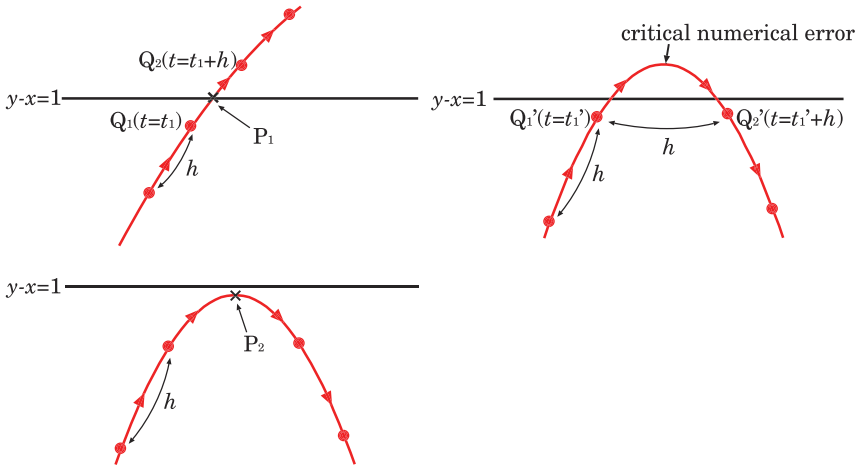

Fig. 3. Important points for the application of piecewise linear explicit solutions with integration step-size h. (a) Upper left: case where a piecewise linear solution is connected without problems. (b) Upper right: case where a piecewise solution with a step-size h is not connected successfully. This causes a critical numerical error. (c) Lower left: our code avoids the critical numerical error shown in the upper right case. The code always monitors the extrema of $y - x$ (P_2 in the figure) to avoid such errors.

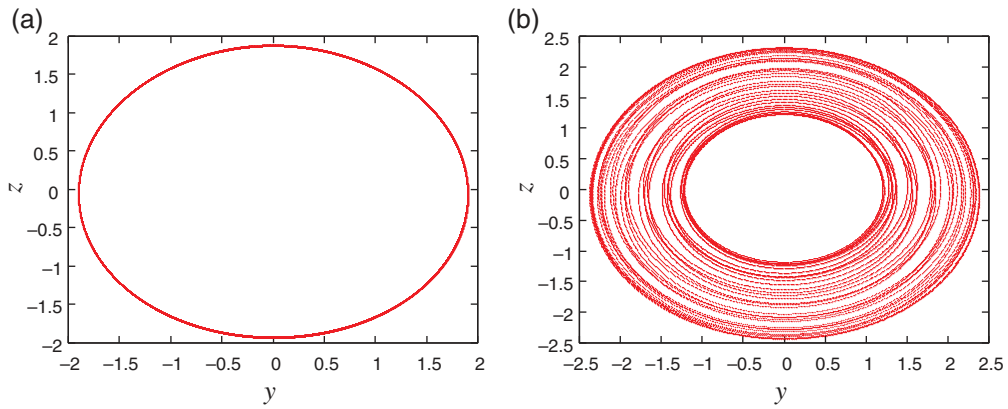

Fig. 4. Trajectory of attractors projected onto the $y - z$ plane when no perturbation is applied. (a) Left: limit cycle ($B = 0, \alpha = 0.5$). (b) Right: two-torus ($B = 0, \alpha = 3$).

Because the perturbation is periodic, the Poincaré map is naturally defined as follows.

$$\begin{aligned} &T_\delta : R^3 \to R^3 \\ &(x, y, z)^\top \mapsto T_\delta(x, y, z)^\top = \varphi(2\pi/\omega;\ (x, y, z)^\top,\ \delta), \end{aligned} \tag{3.1}$$

where the superscript $\top$ denotes the transpose of the vector, $\varphi(t; (x, y, z)^\top, \delta)$ is the solution for which $(x, y, z)^\top$ is the initial condition, and δ is the parameter set. To calculate the Lyapunov exponents, the variational equations must be derived and evaluated, and are represented as follows.
If $y - x > 1$ (Region 1)

$$\dot{\delta x} = \alpha a(\delta y - \delta x), \quad \dot{\delta y} = a(\delta y - \delta x) - \delta z, \quad \dot{\delta z} = \beta \delta y,$$

If $|y - x| \leq 1$ (Region 2)

$$\dot{\delta x} = -\alpha b(\delta y - \delta x), \quad \dot{\delta y} = -b(\delta y - \delta x) - \delta z, \quad \dot{\delta z} = \beta \delta y, \tag{3.2}$$

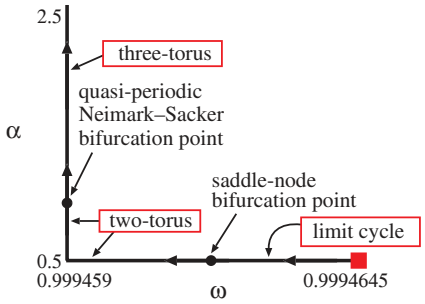

Fig. 5. Direction in which the bifurcation parameter is varied.

If $y - x < 1$ (Region 3)

$$\dot{\delta x} = \alpha a(\delta y - \delta x), \quad \dot{\delta y} = a(\delta y - \delta x) - \delta z, \quad \dot{\delta z} = \beta \delta y,$$

where δx, δy, and δz are variations. Because Eqs. (3.2) are also piecewise linear, the explicit solution can be obtained in a manner similar to the case of Eq. (2.4).

In fact, T_δ and its Jacobian matrix can be theoretically represented by the exact expression because we employ the piecewise linear explicit solutions of Eqs. (2.4) and (3.2). Bifurcation equations are solved with an accuracy of 10^{-15} as shown below. However, it is impractical to express T_δ and its Jacobian matrix explicitly in terms of equations because their domain is separated by Regions 1, 2, and 3. Furthermore, the solution begins at $t = 0$ and wanders throughout these regions until it returns to the initial position at $t = 2\pi/\omega$.

To investigate the bifurcation scenario, we first select an angular frequency for the periodic perturbation equal to the natural angular frequency of the oscillator in the absence of perturbations. In this case, the oscillator is naturally synchronized to the forcing term. We select the following value as the amplitude of the periodic perturbation:

$$B = 0.000\,01. \tag{3.3}$$

Matsumoto et al. successfully observed chaos induced by the torus breakdown in the laboratory measurements [20]. However, B is required to be small in the numerical experiments because the solution tends to diverge for larger values of B near the Neimark–Sacker bifurcation of the limit cycle.

We vary the bifurcation parameter in the direction illustrated in Fig. 5. We set the initial parameters to $\omega = 0.999\,4645$ and $\alpha = 0.5$, corresponding to the point marked with □ (red) in Fig. 5. The three eigenvalues in the complex plane for this initial parameter set are illustrated in Fig. 6. The absolute value of these three eigenvalues is slightly less than 1. In this way, synchronization of the oscillator to the forcing term was confirmed by setting the parameters to appropriate values.

Figure 7(a) shows a stable fixed point that corresponds to a limit cycle of the original Eq. (2.4). Figures 7(b) and (c) are explained later in the paper.

First, we consider ω as the bifurcation parameter. As shown in Fig. 5, when ω decreases, the system is desynchronized. This bifurcation is identified as a saddle-node bifurcation [22] because the real eigenvalue of the Poincaré map T_δ at the fixed point is $0.999\,99\ldots$ when $\omega = 0.999\,4618$. In addition, the fixed point at $\omega = 0.999\,4617$ cannot be traced, which is $0.000\,0001$ less than the previous parameter value of ω, because the fixed point disappears at this parameter value ω via the saddle-node bifurcation. The Poincaré map T_δ and its Jacobian matrix are expressed by the exact equations with an

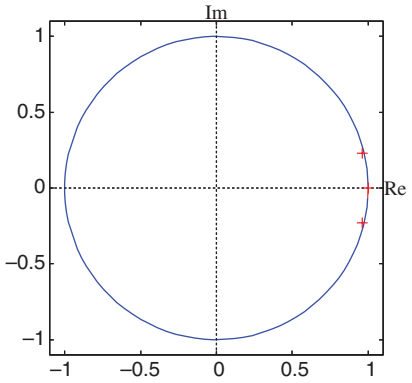

Fig. 6. Location of three eigenvalues in the complex plane with initial parameter values ($\omega = 0.999\,4645$, and $\alpha = 0.5$).

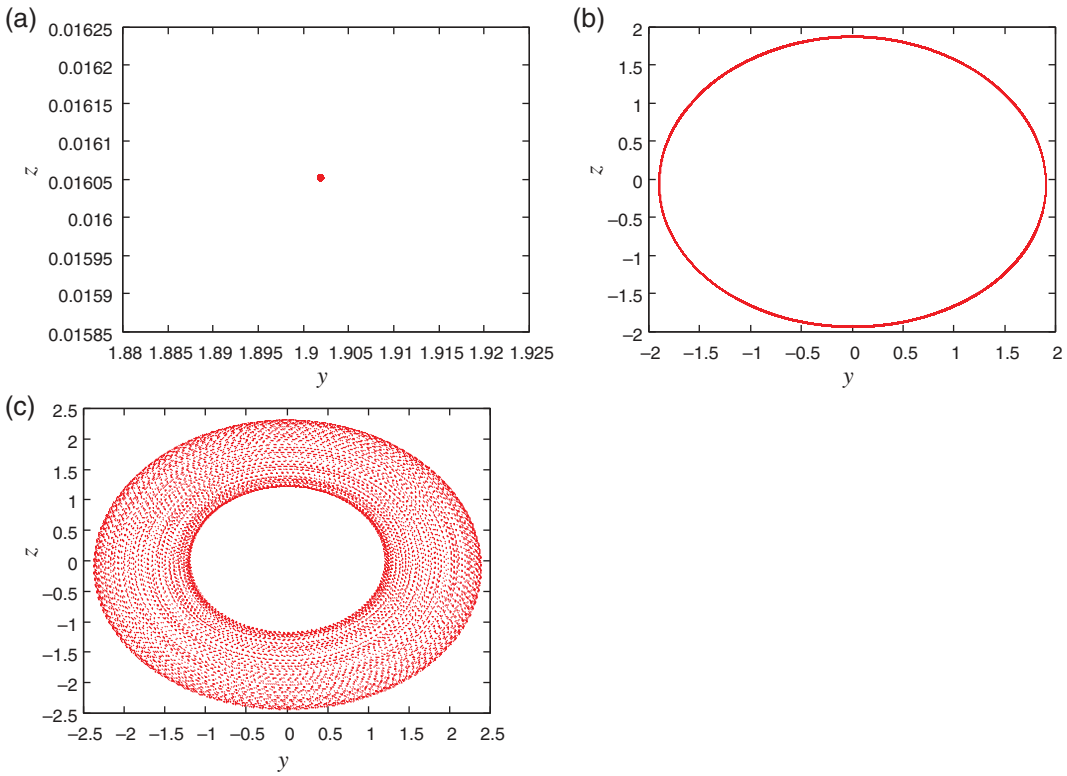

Fig. 7. Attractors on the Poincaré section projected onto the $y-z$ plane. (a) Upper left: stable fixed point that corresponds to the limit cycle ($\omega = 0.999\,4645, \alpha = 0.5$). (b) Upper right: two-torus ($\omega = 0.999\,459, \alpha = 0.5$). (c) Lower left: three-torus ($\omega = 0.999\,459, \alpha = 3$).

accuracy of 10^{-15}; this enables exact evaluation. A conceptual sketch of this situation is illustrated in Fig. 8. After desynchronization via the saddle-node bifurcation, the solution represents a two-torus. Figure 9(a) shows the graph of the largest Lyapunov exponent, and Fig. 9(b) presents the graph of the second and third Lyapunov exponents. These Lyapunov exponents are calculated by using a procedure presented by Shimada and Nagashima [23]. After the saddle-node bifurcation, the attractor is identified to be a two-torus because the largest Lyapunov exponent λ_1 is zero. Figure 7(b) presents the two-torus. Because the Poincaré section forms an invariant closed curve, the attractor is quasi-periodic. Because two of the eigenvalues of the Poincaré map form a pair of complex conjugates, the

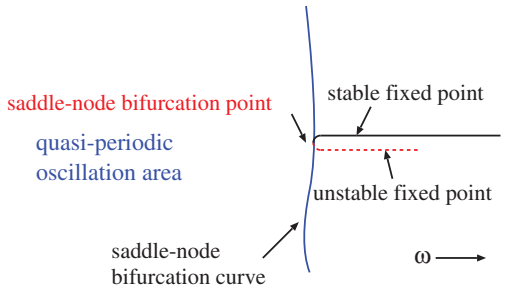

Fig. 8. Conceptual sketch of fixed-point manifold and saddle-node bifurcation.

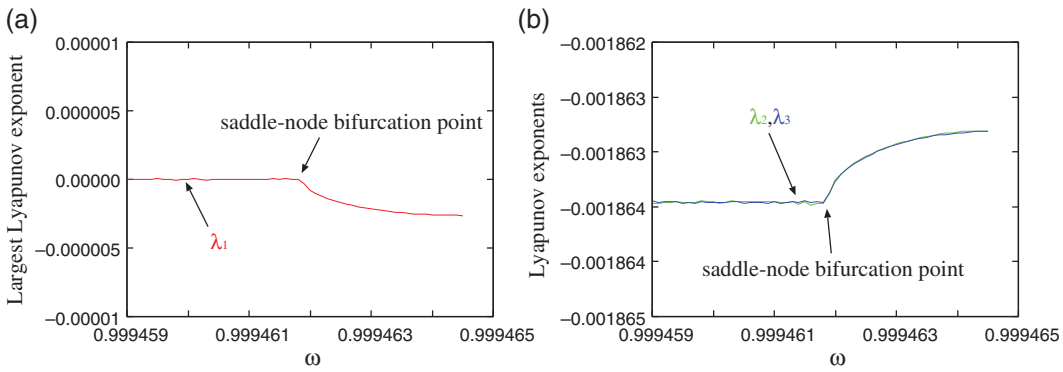

Fig. 9. Graph of Lyapunov exponents. (a) Left: largest Lyapunov exponent ($B = 0.000\,01$, $\alpha = 0.5$). (b) Right: second and third Lyapunov exponents ($B = 0.000\,01$, $\alpha = 0.5$).

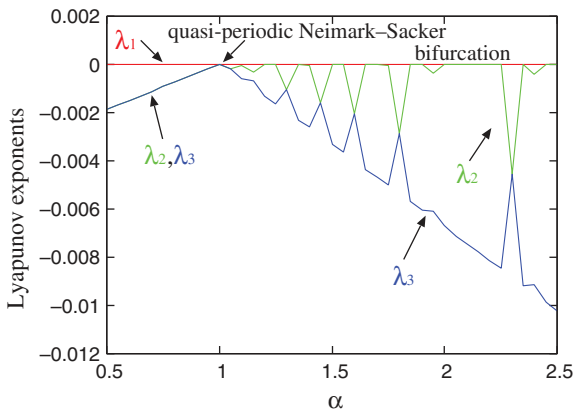

Fig. 10. Graph of Lyapunov exponents ($B = 0.000\,01$, $\omega = 0.999\,459$).

second and third Lyapunov exponents are degenerate. This suggests that, even after the saddle-node bifurcation, the pair of complex eigenvalues retains its nature after the fixed point disappears.

Next, we set $\omega = 0.999\,459$ and select a bifurcation parameter, as depicted in Fig. 5. We vary α in the direction shown in Fig. 5. Figure 10 shows the graph of the Lyapunov exponents. In Fig. 10, a quasi-periodic Neimark–Sacker bifurcation occurs at the point labeled "quasi-periodic Neimark–Sacker bifurcation." This bifurcation is identified as the quasi-periodic Neimark–Sacker bifurcation because, before the bifurcation point, the largest Lyapunov exponent is zero ($\lambda_1 = 0$), and the second and third Lyapunov exponents are negative and degenerate ($\lambda_2 = \lambda_3 < 0$) [5,12]. Furthermore, after this bifurcation, λ_2 becomes zero, and λ_3 becomes negative. This behavior of the Lyapunov exponents is the distinctive property of a quasi-periodic Neimark–Sacker bifurcation [5,12].

A three-torus cannot necessarily be generated by a Neimark–Sacker bifurcation and a quasi-periodic Neimark–Sacker bifurcation [5,12,16] in the forced oscillator. Figure 7(c) shows the Poincaré section of a three-torus via a saddle-node bifurcation and a quasi-periodic Neimark–Sacker bifurcation.

After the quasi-periodic Neimark–Sacker bifurcation, the second Lyapunov exponent λ_2 in Fig. 10 frequently becomes negative. This phenomenon is considered to be a two-torus Arnold tongue [12]. The two-torus Arnold tongue refers to a bifurcation structure in which many two-torus-generating regions exist in the three-torus-generating region, which is similar to the case of periodic states existing in a two-torus-generating region in an Arnold tongue.

4. Conclusion

In this study, a three-torus generated in a third-order piecewise linear oscillator under a weak periodic perturbation was investigated. Because a three-torus cannot be generated in third-order ordinary autonomous differential equations, the proposed oscillator could exhibit a three-torus of minimal dimension. Appropriate initial parameter values were selected to synchronize the oscillator to the weak periodic perturbation by equalizing the frequency of the forcing term to the natural frequency of the autonomous oscillator. It was confirmed that a limit cycle bifurcated to a two-torus via a saddle-node bifurcation. Furthermore, the two-torus bifurcated to a three-torus via a quasi-periodic Neimark–Sacker bifurcation.

Acknowledgments

This work was supported by MEXT/JSPS KAKENHI Grant Number 24560556.

References

[1] K. Mitsubori and T. Saito, IEEE Trans. Circuits Syst. I **41**, 782 (1994).
[2] N. Inaba, Y. Nishio, and T. Endo, Physica D **240**, 903 (2011).
[3] T. Suzuki and T. Saito, IEEE Trans. Circuits Syst. I **41**, 876 (1994).
[4] T. Saito and Y. Matsumoto, IEEE Trans. Circuits Syst. I **41**, 754 (1994).
[5] K. Kaneko, Prog. Theor. Phys. **71**, 282 (1984).
[6] C. Baesens, J. Guckenheimer, S. Kim, and R. S. MacKay, Physica D **49**, 387 (1991).
[7] O. Hess, D. Merbach, H. Herzel, and E. Schöll, Phys. Lett. A **194**, 289 (1994).
[8] Y. A. Kuznetsov, *Elements of Applied Bifurcation Theory* (Springer, New York, 2004), 3rd ed., Chap. 8.
[9] J. M. Lopez and F. Marques, Phys. Rev. E **68**, 036302 (2003).
[10] J. M. Lopez and F. Marques, Phys. Rev. Lett. **85**, 972 (2000).
[11] C. Giberti and R. Zanasi, Physica D **65**, 300 (1933).
[12] M. Sekikawa, N. Inaba, T. Tsubouchi, and K. Aihara, Physica D **241**, 1169 (2012).
[13] N. Inaba, M. Sekikawa, and T. Endo, Nonlinear Theor. Appl. **3**, 508 (2012).
[14] D. J. Albers and J. C. Sprott, Physica D **223**, 194 (2006).
[15] H. T. Moon, P. Huerre, and L. G. Redekopp, Phys. Rev. Lett. **49**, 458 (1982).
[16] R. Alaggio and G. Rega, Physica D **137**, 70 (2000).
[17] I. Manimehan, K. Thamilmaran, and P. Philominathan, Int. J. Bifurcation Chaos **21**, 1987 (2011).
[18] R. Vitoro, H. Broer, and C. Simo, Regul. Chaotic Dyn. **16**, 154 (2011).
[19] S. Fujiwara, N. Inaba, M. Sekikawa, K. Fujimoto, and T. Yoshinaga, The Institute of Electronics, Information and Communication Engineers (IEICE), Nonlinear Problems **2012-159**, 77 (2013) [in Japanese].
[20] T. Matsumoto, L. O. Chua, and R. Tokunaga, IEEE Trans. Circuits Syst. **34**, 240 (1987).
[21] Y. Nishiuchi, T. Ueta, and H. Kawakami, Chaos Solitons Fractals **27**, 941 (2006).
[22] H. Kawakami, IEEE Trans. Circuits Syst. **31**, 248 (1984).
[23] I. Shimada and T. Nagashima, Prog. Theor. Phys. **61**, 1605 (1979).